Conceptual Design of a Tiltduct Reference Vehicle for Urban Air Mobility

Siena K. S. Whiteside Aerospace Engineer
Beau P. Pollard Aerospace Engineer
NASA Langley Research Center
Hampton, VA, USA

ABSTRACT

NASA is establishing a fleet of conceptual air vehicle designs to support research and development for Urban Air Mobility (UAM). This fleet of vehicles will enable examination of the sensitivity of UAM vehicle designs to technology assumptions, identify key research and development needs for UAM aircraft, and provide the UAM community with reference vehicles that are publicly available and based upon known assumptions. To date, five six-passenger UAM reference vehicles have been published: a single-main-rotor helicopter, a side-by-side helicopter, a quadrotor, a lift-plus-cruise, and a tiltwing. To increase the breadth of vehicle technologies encapsulated in the fleet of NASA UAM reference vehicles, this paper establishes a tiltduct vehicle as an addition to the fleet. The fleet will continue to evolve as future analyses and trade studies are performed.

The tiltduct UAM reference vehicle has six tilting ducted proprotors. This paper describes the initial configuration downselection; discusses ducted proprotor design rules of thumb as they applied to the conceptual design of the reference vehicle; describes the vehicle sizing, trade studies, and tuning of models performed; and finally, compares the resulting tiltduct vehicle against the other six-passenger NASA UAM reference vehicles. The high-level analyses performed for this study did not indicate significant differences in performance between the tiltduct and tiltwing reference vehicles, and so vehicle performance alone may not be a key driver in the selection of a tiltduct vehicle over a tiltwing vehicle. However, if ducts are found to have significant acoustical benefits, then acoustical priorities may provide a compelling reason to incorporate ducted proprotors.

One significant limitation of the design presented in this paper is that the ducted proprotor performance was tuned based upon performance characteristics observed during historical tests with disk loadings (defined as thrust divided by proprotor disk area) of 125-250 lb/ft^2. The tiltduct vehicle designed in this study has a disk loading of 30 lb/ft^2, to be more representative of UAM vehicles; further studies to understand performance of ducted proprotors at representative disk loadings are warranted.

NOTATION

A_e	Duct exit area, ft^2
A_R	Proprotor disk area, ft^2
$\mathcal{AR}$	Aspect ratio
C_{D_i}	Induced drag coefficient
C_L	Lift coefficient
$C_{P_{cruise}}^{est}$	Calculated cruise power coefficient from Ref. 24
$C_{P_{hover}}^{est}$	Calculated hover power coefficient from Ref. 24
$C_{P_{cruise}}^{NDARC}$	NDARC-calculated cruise power coefficient
$C_{P_{hover}}^{NDARC}$	NDARC-calculated hover power coefficient
C_T	Thrust coefficient
D	Distance, nmi
d	Proprotor diameter, ft
L/D_e	Equivalent lift-to-drag ratio, $L/D_e = WV_{br}/P$
l_{duct}	Duct chord length, ft
n	Proprotor rotational speed, rev/s
P	Power, hp
P_i	Induced power, ft-lb/s
P_{ideal}	Ideal power, ft-lb/s
ST	Specific torque, ft-lb/lb
T	Thrust, lb
t	Time, s
U_{duct}	Duct weight per area, lb/ft^2
V	Airspeed, ft/s
V_{br}	Airspeed for best range, ft/s
V_y	Airspeed for best rate of climb, ft/s
W	Weight, lb

Presented at the VFS Aeromechanics for Advanced Vertical Flight Technical Meeting, San Jose, CA, Jan 25-27, 2022.

α	Angle of attack, deg
η_{cruise}	Cruise efficiency
η_{hover}	Hover efficiency
κ_i	Induced power multiplier
ρ	Air density, slugs/ft^3
σ_d	Duct area ratio, $\sigma_d = A_e/A_R$
τ	Torque, ft-lb
χ	Tech factor applied in NDARC

INTRODUCTION

This paper is part of a series of publications that explore vehicle requirements and technology trades for Urban Air Mobility (UAM). The ultimate objectives of this series of papers are to establish a catalog of conceptual air vehicle designs, referred to as "NASA UAM reference vehicles," examine the sensitivity of these vehicle designs to technology assumptions, and identify key research and development needs for UAM aircraft. Across the UAM community, a wide range of UAM vehicle configurations and operational missions have been proposed. The fleet of NASA UAM reference vehicles aims to be representative of many of the vehicle configurations proposed across the UAM community, without specifically replicating any single industry solution.

In January 2018, Johnson et al. published designs of three concept vehicles for vertical takeoff and landing (VTOL) air taxi operations (Ref. 1). These concepts included an electric single-passenger quadrotor, a hybrid-electric six-passenger side-by-side helicopter, and a turboelectric fifteen-passenger tiltwing concept. Then, in May 2018, Patterson et al. defined a set of UAM mission requirements (Ref. 2). The most constraining mission identified by Patterson et al. included transporting six passengers on two 37.5 nautical mile "hops" without refueling/recharging. This most-constraining mission was used to resize two of the existing VTOL air taxi concepts by Johnson et al., the quadrotor and side-by-side helicopter, and also to design a new turboelectric lift-plus-cruise concept vehicle, published by Silva et al. in June 2018 (Ref. 3). All subsequent NASA UAM reference vehicles to date have been sized for this same, most-constraining, six-passenger mission.

In January 2019, Antcliff et al. examined the technology assumptions made during the design of the existing concept vehicles and discussed potential future technologies that were not yet included in the reference vehicle designs (Ref. 4). In January 2020, Johnson published a single-main-rotor helicopter concept vehicle designed specifically for low-noise operations utilizing demonstrated technologies, to serve as a baseline for comparison with existing and future UAM reference vehicles which require one or more novel technologies (Ref. 5). Then, in June 2021, Whiteside et al. published a turboelectric tiltwing vehicle design, implementing updated technology assumptions, and compared the new tiltwing vehicle with an updated lift-plus-cruise vehicle that utilized the same assumptions (Ref. 6).

To increase the breadth of vehicle technologies encapsulated in the fleet of NASA UAM reference vehicles, this paper establishes a tiltduct vehicle as an addition to the fleet. The fleet of NASA UAM reference vehicles, including the tiltduct reference vehicle described in this paper, is shown in Figure 1. The fleet will continue to evolve and subsequent versions of the reference vehicles will be based upon the results of future trade studies and technology developments.

A tiltduct is a compelling aircraft type for study because the ducts have the potential to reduce, shield, and/or redirect noise, improve aerodynamic performance, mitigate the effects of blade-off events, improve safety during ground handling, and potentially improve public perception due to the lack of open rotors or propellers. There are several known technology challenges and opportunities which exist for tiltduct vehicles, and this reference vehicle will allow researchers to explore the challenges (for example, separation effects at the duct lip) and opportunities (for example, noise reduction) associated with tiltduct UAM vehicles.

This paper briefly describes the mission requirements and the tools leveraged for the design of the tiltduct. Then, it details the design process that was followed, including the initial vehicle configuration design, design decisions specific to ducted proprotors, and vehicle design refinement including vehicle sizing trades. The resulting tiltduct UAM reference vehicle, which uses a turboelectric propulsion system to power six proprotors positioned inside tilting ducts, is then compared with the other NASA six-passenger UAM reference vehicles, and important limitations of the design are discussed. The paper closes with concluding remarks based on the findings of this initial design of a tiltduct UAM reference vehicle.

SIZING MISSION

This work used the most constraining of the mission requirements set out by Patterson et al. (Ref. 2) in order to be consistent with the previous concepts developed by Silva et al. (Ref. 3). Figure 2 represents the sizing mission in height above ground level (AGL), assuming a takeoff and landing altitude of 6,000 ft international standard atmosphere (ISA). The mission represented in Figure 2 consists of two identical 37.5 nautical mile "hops" into a headwind of 10 knots (segments 1-9 and 10-18) and a 20 minute cruise reserve (segment 19). Table 1 details segments 1-9 (which are identical to segments 10-18) and segment 19 (cruise reserve). The variables denoted in the table are determined by sizing the vehicle based on speeds for best rate of climb, V_y, and best range, V_{br}, for the climb and cruise segments, respectively.

In addition to the main sizing mission, the reference vehicles are sized for a second sizing mission and two performance conditions are established. The second sizing mission achieves emergency sizing of the propulsion battery system by requiring the vehicle to hover for two minutes at hover out-of-ground effect (HOGE) power (roughly equivalent to a discharge rate of 30C); the batteries are expected to be used only once for this contingency, and battery replacement is assumed to be necessary after this event. The first performance

(a) Single-main-rotor helicopter (b) Side-by-side helicopter (c) Quadrotor

(d) Lift-plus-cruise (e) Tiltwing (f) Tiltduct

Figure 1: Six-passenger NASA UAM reference vehicles.

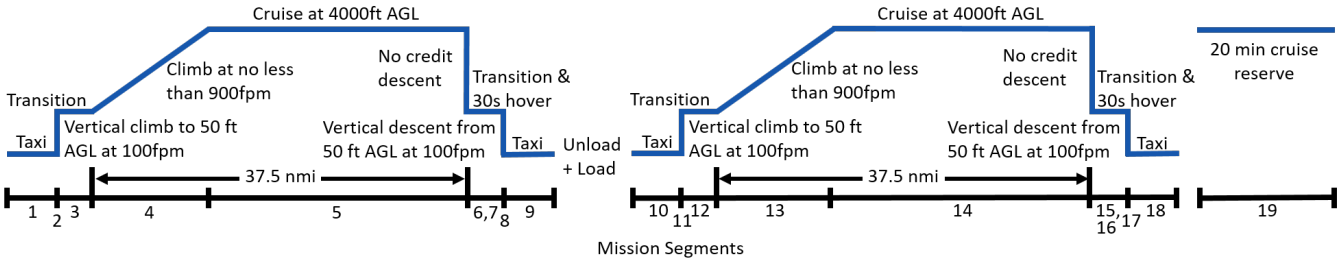

Figure 2: Sizing mission profile representing two identical "hops" and a 20 minute cruise reserve.

Table 1: Sizing Mission Segments 1-9 and 19, and Their Associated Properties

Segment	1	2	3	4	5	6	7	8	9	19
Initial altitude (ft MSL ISA)	6,000	6,000	6,050	6,050	10,000	6,050	6,050	6,050	6,000	10,000
Final altitude (ft MSL ISA)	6,000	6,050	6,050	10,000	10,000	6,050	6,050	6,000	6,000	10,000
Time (s)	15	30	10	t_{climb}	t_{cruise}	10	30	30	15	1200
Distance (nmi)	-	0	0	D_{climb}	37.5-D_{climb}	0	0	0	0	-
Airspeed	-	-	0	V_y	V_{br}	0	0	-	-	V_{br}
Rate of climb (ft/min)	-	100	0	≥ 900	0	0	0	-100	-	0
Percent of max power	10%	100%	100%	P_{climb}	P_{cruise}	100%	100%	100%	10%	P_{cruise}

condition determines the maximum takeoff weight (MTOW) of the vehicle by performing HOGE at 6,000 ft ISA at 100% maximum rated power (MRP). The second performance condition ensures that the vehicle can execute a cruise climb of at least 500 ft/min at 10,000 ft ISA, at $\leq$100% MRP and design gross weight.

TOOLS

The primary sizing and performance analysis tool utilized in this study was NASA Design and Analysis of Rotorcraft (NDARC) release 1.15c (Ref. 7). NDARC is an aircraft system analysis tool intended to support both conceptual design efforts and technology impact assessments. The principal function of NDARC is to size an aircraft to meet specified design conditions and missions and then analyze the performance of the aircraft for a set of off-design missions and operating conditions. The aircraft is modeled as a set of components, such as fuselage, rotors, wings, tails, gearboxes, and drive shafts. For each component, attributes such as performance, drag, and weight can be estimated. The aircraft attributes are obtained from the aggregation of the component attributes. NDARC enables trade studies to be quickly and consistently performed; for example, NDARC enables the evaluation of potential benefits and drawbacks of many different technologies and the impacts of modifications to mission requirements on the whole aircraft's design and performance.

NDARC was first written incorporating low-fidelity models appropriate for general rotorcraft conceptual design, but was designed to be broadly adaptable to conventional and unconventional aircraft concepts; the architecture of the NDARC code accommodates configuration flexibility, a hierarchy of models, and ultimately, multidisciplinary design, analysis, and optimization. Currently, NDARC provides a capability to estimate the performance and attributes of advanced concepts through models which have been added to meet specific research goals. Development and incorporation of additional models in NDARC will be driven by the needs of the researchers investigating technology trades on the NASA UAM reference vehicles.

For the results presented in this paper, NDARC was executed via An Integrated Design Environment for NDARC (AIDEN) version 2.0.6 (Ref. 8). AIDEN improves the NDARC user input and output experience by providing a graphical user interface and introducing syntax checking, input auto-completion, model version control, and other data entry and management tools similar to those found in integrated development environments. The designer's ability to interpret output is improved through a set of tools that display solution convergence information, provide an indexed form of NDARC output, and automate plot generation.

OpenVSP, an open-source parametric geometry tool (Ref. 9), was used to generate conceptual models both for visualization and modeling. OpenVSP models can be generated and updated directly from NDARC outputs using an "N2 event" in AIDEN: an N2 event allows the user to couple NDARC jobs and Python scripts (Ref. 10); Python scripts can directly update OpenVSP geometries by utilizing the Python-to-OpenVSP application programming interface (API). OpenVSP geometry models are then available as a basis for further aircraft design studies, such as aerodynamic and structural analyses, and the results obtained can be fed back into NDARC.

INITIAL CONFIGURATION DESIGN

This section describes the initial configuration exploration and downselection that was performed. First, in order to gain an understanding of the tiltduct vehicle concepts that had been proposed to date, a survey was performed of some 30-40 historical and recent aircraft concepts that incorporated tilting ducted propellers, fans, or rotors. The aircraft concepts surveyed each had between two and 36 tilting ducts.

Some of the concepts surveyed incorporated other propulsion methods in addition to tilting ducts, most notably lift fans. Lift fans may show promising benefits especially when embedded in a wing (Ref. 11); however, for simplicity of future design trades, it was decided that the NASA tiltduct UAM reference vehicle would utilize only one major distinguishing technology, tilting ducts, with no lift fans.

Additionally, some of the concepts surveyed included many small tilting ducts aligned along the span of the wing; for example, the Lilium Jet incorporates many tilting ducts to augment lift over the wing (Ref. 12), and the Aurora Flight Sciences XV-24A LightningStrike incorporates many ducts integrated along the span of a tilting wing (Ref. 13). For the purposes of the NASA tiltduct UAM reference vehicle and anticipated future research applications, fewer, larger tilting ducts were desired.

Next, initial configuration sketches were made of potential tiltduct configurations. This first reference vehicle would be designed with a turboelectric propulsion system, with the potential to resize to an all-electric version at a later date. All ducts on an individual vehicle were chosen to have the same diameter, to ease manufacturing and maintenance burden. Disk loading, defined as thrust per proprotor disk area, $\frac{T}{A_R}$, was maintained at approximately 30 lb/ft^2 assuming a gross weight of 6500 lb. A disk loading of 30 lb/ft^2 was selected simply as an initial starting value to target a hover power and downwash velocity similar to other UAM vehicles with open rotor disk loadings of about 15 lb/ft^2. Trades on disk loading were performed later in the design study.

Lateral and vertical spacing of the ducts was targeted to reduce wake interference. For many configurations, lateral separation of the ducts was achieved by mounting ducts on a long strut or fixed wing; a fixed wing would also aid in producing lift during cruise flight but could complicate vehicle performance during VTOL aspects of the mission. Four general configurations were selected for further consideration; each had between four and eight tilting ducts and their OpenVSP geometries are represented in Figure 3.

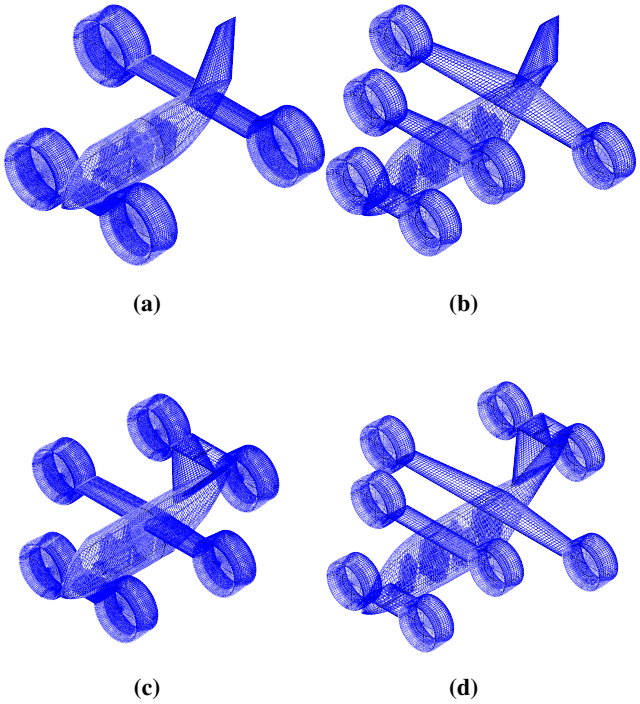

Figure 3: Early tiltduct configuration exploration: four potential configurations (cruise configuration shown).

Relative to open (unducted) proprotors, the ducts installed on ducted proprotors contribute a large wetted area and therefore parasite drag. It is important to maximize cruise speed for most UAM business cases (to maximize travel time savings), and parasite drag may limit cruise speed and/or efficiency. Interestingly, however, total duct wetted area did not influence the configuration downselect. With disk loading and the ratio of duct diameter to duct chord length consistent between each configuration, the total duct wetted area on each vehicle does not vary between the four-, six-, and eight-ducted configurations considered here.

The configuration with four ducts, shown in Figure 3a, is similar to the X-22A configuration (Ref. 14); it has two ducts mounted in a canard location and two ducts mounted at the tip of a main wing towards the rear of the aircraft. A comprehensive description of the conceptual design study that led to the X-22A 4-duct configuration is described in Ref. 14, so additional iterations on four-duct configurations are not presented here. The X-22A design process briefly considered cross-shafted configurations with two, three, four, or five ducts and the decision to utilize four ducts on the X-22A was a result of engine weight and availability, while considering the thrust-to-weight ratio required for one-engine-out hover capability. With the availability today of distributed electric propulsion, which has the potential to offer a lighter weight solution and more flexibility in propulsion system architecture, a majority of UAM concepts presented by the UAM community utilize greater than four propulsors, and so the focus was shifted to concepts with greater than four ducts for this design study.

For the configurations represented in Figures 3b and 3d, it was challenging to achieve vertical separation so as to prevent ducted proprotor wake impinging on a wing. Wake impinging on the wing is a concern for aerodynamic performance and is a potential noise source. Both of these configurations have a main wing supporting the third pair of ducts, which is located directly behind the second pair of ducts (pairs of ducts are defined as two ducts positioned at the same longitudinal point on the vehicle; pairs are counted longitudinally from the front).

The configuration with six ducts and a central main wing, shown in Figure 3c, achieves vertical and lateral separation of the ducts, minimizing interference effects during cruise while having a smaller, and therefore lighter weight, main wing than the other six-duct configuration and the eight-duct configuration. In hover mode, this six-duct configuration with a central main wing has ducts positioned approximately co-radially about the center of gravity, providing a thrust distribution that lessens the need to oversize the propulsors for a significant loss of thrust event. This configuration potentially also provides more flexibility for passenger ingress/egress solutions by keeping the second and third pairs of ducts laterally and vertically farther from the fuselage.

Ultimately, the six-duct configuration with a central main wing was selected as the configuration to continue to explore during the design process presented in this paper.

DUCT DESIGN DECISIONS

Following selection of the general configuration of the vehicle, focus moved to design of the ducted proprotors, since these were the unique aspect of the vehicle that had not been modeled in previous NASA UAM reference vehicles. A literature review was performed to understand ducted proprotor aerodynamics and to explore the current state-of-the-art in tilting duct design for VTOL vehicles. Design insights and rules of thumb were attained from performance characteristics predicted by momentum theory and observed in historical wind tunnel and flight tests. Furthermore, for the purposes of sizing the vehicle in NDARC, it was necessary to ensure that the performance and weight of the ducts modeled in NDARC were realistic.

This section first provides a summary of ducted proprotor aerodynamics as they applied to conceptual design of this tiltduct UAM reference vehicle, and then a brief discussion on acoustical considerations. Next, the design decisions related to the selection of the ducted proprotor geometry for this vehicle are discussed. Finally, adjustments that were made to the vehicle model in NDARC to account for duct lift at small angles of attack are described, and then duct weight estimation is described.

Ducted Proprotor Aerodynamics

The performance of a ducted proprotor relative to an open proprotor can be considered from a momentum theory perspective (Refs. 15–17), revealing some general insights about ducted proprotor performance as it applies to conceptual design. For an open proprotor, the downstream proprotor wake contracts to half of the proprotor disk area. On the other hand, for a ducted proprotor, the duct constrains the wake streamlines to follow the duct surface and to exit at a velocity determined by the duct exit area[1], assuming that the flow does not separate from the duct surface. The duct area ratio, σ_d, is defined as:

$$\sigma_d = \frac{A_e}{A_R} \tag{1}$$

where A_R is the proprotor disk area and A_e is the duct exit area. Note that for an open proprotor, the effective area ratio is 0.5 since the proprotor wake contracts to half of the proprotor disk area. For a typical ducted proprotor, σ_d is often close to or greater than 1. Note also that although σ_d is used in the following discussion, the absolute thrust and power of a ducted or open proprotor are independent of A_R, and are determined by the downstream wake area and velocity.

Hover

Momentum theory provides that the induced power in hover of a ducted or open proprotor is:

$$P_i = \frac{T^{3/2}}{2\sqrt{\sigma_d \rho A_R}} \tag{2}$$

[1]Note that the diffuser angle of the duct may encourage flow to expand further, downstream of the duct exit, thereby further increasing the wake area (Ref. 18).

where T is the thrust produced by the ducted or open proprotor.

If thrust and proprotor diameter are maintained constant between the open proprotor and ducted proprotor, then the induced power of the ducted proprotor, $P_{i,ducted}$, is:

$$P_{i,ducted} = \frac{1}{\sqrt{2\sigma_d}} P_{i,open} \tag{3}$$

where $P_{i,open}$ is the induced power of the open proprotor. Therefore, if σ_d is close to 1, then the induced power required by the ducted proprotor is close to 71% of the induced power required by the open proprotor. Additionally, the wake velocity induced by the ducted proprotor is reduced by a factor of $\sqrt{2\sigma_d}$ relative to an open proprotor, thereby reducing downwash velocity and wind effects on the ground during departure and arrival.

If, instead, thrust and induced power are maintained constant between the open proprotor and ducted proprotor[2], for example, to determine the open or ducted proprotor diameter required for a vehicle of fixed weight and power, then the required diameter of the ducted proprotor, d_{ducted}, is:

$$d_{ducted} = \frac{1}{\sqrt{2\sigma_d}} d_{open} \tag{4}$$

where d_{open} is the diameter of the open proprotor. If σ_d is close to 1, then the required ducted proprotor diameter is close to 71% of the diameter of an equivalent open proprotor. Additionally, if the disk loading of the ducted proprotor in hover is defined as $\frac{T}{A_{R,ducted}}$, then:

$$\frac{T}{A_{R,ducted}} = 2\sigma_d \frac{T}{A_{R,open}} \tag{5}$$

where $\frac{T}{A_{R,open}}$ is the disk loading of the open proprotor. Since disk loading is commonly referenced when comparing vehicle configurations, and σ_d is often close to 1, then for the purposes of conceptual design comparisons with open proprotors, the "equivalent" disk loading of a ducted proprotor can be thought of as being close to half of what it would be if the proprotor was not ducted. For example, if the disk loading of a ducted proprotor, $\frac{T}{A_{R,ducted}}$, is 30 lb/ft^2, then that ducted proprotor provides an equivalent thrust, induced power, and slipstream velocity to an open rotor with close to half the disk loading (15 lb/ft^2).

It is apparent from the equations above that the hover performance of a duct will increase with area ratio, σ_d, as long as the duct chord length, l_{duct}, is sufficient to maintain a diffuser ratio, σ_d / l_{duct}, that prevents flow separation from the inner surface of the duct. Furthermore, it is desirable that there is no flow separation over the inlet lip of the duct; therefore, design of the duct inlet lip for static conditions tends to lead to a relatively large inlet lip radius, and a relatively thick duct cross section.

[2]Note that fixing thrust and induced power is equivalent to fixing the downstream wake area and wake velocity.

Axial forward flight

Momentum theory can be extended to predict axial forward flight of ducted proprotors, again provided that there is not flow separation inside the duct. If a duct is designed for hover conditions, and has a fixed geometry, then as axial airspeed increases, the proprotor wake will begin to separate from the duct walls upstream of the duct exit. At high axial forward flight speeds, the thrust and power benefits that were seen in hover reduce such that the ducted proprotor behaves similar to an open proprotor, except with the added weight and drag of the duct (i.e., the component of thrust due to the duct goes negative).

A ducted proprotor can be designed to perform close to the theoretical maximum predicted by momentum theory, for any desired subsonic axial forward flight speed, as observed by Mort (Ref. 19). Mort evaluated the results of a ducted propeller test that was reported in Ref. 20, and created a plot of thrust efficiency (thrust divided by shaft horse power, SHP) versus axial forward flight speed, shown in Figure 4.

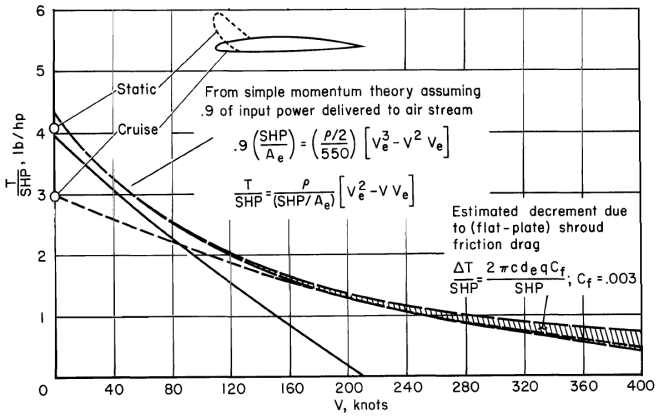

Figure 4: Thrust efficiency versus axial forward flight velocity for two ducted propeller designs ("Static" and "Cruise"), overlaid with momentum theory predictions and a skin friction drag estimate (Ref. 19).

The ducted propeller test reported in Ref. 20 evaluated two different leading-edge configurations: one with a duct inlet designed for high axial forward flight speeds (labeled "Cruise" in Figure 4), and one with a duct inlet designed to provide high static thrust (labeled "Static" in Figure 4). Mort compared the thrust efficiency of the test with that predicted by momentum theory, assuming a 90% efficiency of input power transfer to the air stream. Further, a flat plate drag coefficient was used to estimate skin friction drag, which was decremented from the theoretical thrust efficiency. Mort found that both the ducted propeller designed for static conditions, and the ducted propeller designed for high axial forward flight speeds, showed performance comparable to that predicted theoretically, for their design speed ranges: each ducted propeller followed an almost linear decrease in thrust efficiency with velocity, and was approximately tangential to the predicted curve in the speed range for which it was designed. Therefore, duct geometry can be tailored depending

on the desired axial forward flight speed. However, it is apparent that design of a fixed-geometry ducted proprotor requires a trade between hover and cruise performance, and variable duct geometries may be desirable in order to improve overall mission performance.

Ducts can act somewhat similarly to annular wings in axial forward flight by flying at a small angle of attack to produce lift. Grose (Ref. 20) observed that a portion of ducted propeller lift arises from the component of lift obtained due to propeller thrust (60% for the configuration studied by Grose), and a portion results from an increase in circulation on the duct itself (40% for the configuration studied by Grose). Grose also reported tests of ducted propellers with the propeller blades removed and compared them with a simple rectangular wing having a span equal to the diameter of the duct and chord equal to the duct chord length. The duct was found to produce approximately twice the lift of the rectangular wing and approximately equivalent induced drag[3]. For a ducted fan positioned at the tip of a wing, it has also been observed that interactions between the wing and duct together can produce a larger lift than the sum of the lift of each isolated component, and this effect increased with airspeed (Ref. 21).

Flight at large, non-zero angles of attack

Operation of ducted proprotors at large, non-zero angles of attack will be necessary for VTOL missions. In particular, non-zero angles of attack will occur during transition between cruise and hover, descending flight, and climbing flight. The characteristics of ducted proprotors at non-zero angles of attack were explored via wind tunnel tests of a replica of the 4 ft diameter VZ-4 ducted fan in the early 1960s (Refs. 21–23), and a replica of the 7 ft diameter X-22A ducted propeller later in the 1960s (Ref. 24). The X-22A ducted propeller had a similar duct geometry to that of the VZ-4, except with blade collective control. Note that the disk loadings explored in these tests were approximately 125 to 250 lb/ft^2; the tiltduct UAM reference vehicle described in this paper targets a disk loading close to 30 lb/ft^2. Further studies of reduced disk loadings are desired in order to confirm applicability of these observations down to disk loadings of approximately 30 lb/ft^2.

When operating at a positive angle of attack, ducted proprotors produce a pitch-up moment. Reference 22 explored steady level flight conditions for a transition regime between hover (0 knots) and cruise flight (140 knots) airspeeds, and determined the variation of duct angle, power required, and pitching moment encountered. The pitch-up moment was found to be a maximum at approximately 45 knots, when the duct angle of attack was approximately 60 degrees. The pitching moment was predominantly caused by the moment arm of the normal force produced by the duct shroud, as well as differential thrust on the shroud lips. Furthermore, it was found that the maximum pitching moment increased when disk loading was reduced from 250 to 125 lb/ft^2.

[3]Note that annular wings can theoretically produce twice the lift and half the induced drag of the simple rectangular wing, so there may be scope to reduce induced drag further than described here.

Reference 21 explored the addition of a horizontal exit vane installed across the rear of the duct, with a 25% chord plain flap, and found that it was possible to program the deflection of the exit vane flap so as to enable a wide airspeed range (25 knots and above) during which no change in vehicle trim would be required. Exit vanes provide a potential advantage in that they are positioned in the location of high-energy flow, independent of freestream speed, and they are colocated with the duct and so counteract the pitching moment of the duct about its own axis, rather than requiring additional power elsewhere on the vehicle. The tiltduct UAM reference vehicle configuration in this paper has vertically and longitudinally spaced ducts, and so has additional control freedoms for vehicle pitch trim that may alleviate the need for exit vane control surfaces. For example, the thrust axis of the third row of ducts acts to induce a nose-down pitching moment. Further studies into flight dynamics and control of the tiltduct vehicle, beyond the scope of this paper, will ultimately guide the desirability of exit vanes on this vehicle; for this initial concept, a horizontal exit vane with a 25% chord plain flap is installed in each duct.

Operation of ducted proprotors at large angles of attack is likely to cause flow separation at the leading edge of the duct. In particular, stall of the upstream (lower) lip region, as depicted in Figure 5, is of primary concern because the lower lip is more heavily loaded, so stall of the lower lip would result in a larger reduction in lift. Furthermore, stall of the lower lip is likely to significantly disturb the proprotor inflow, thereby reducing proprotor performance and/or fatigue life and increasing noise.

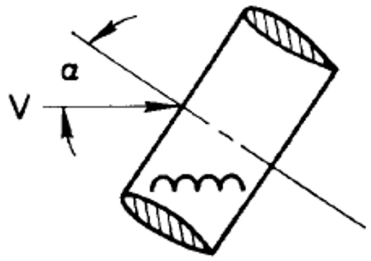

Figure 5: Depiction of upstream (lower) lip separation for a duct at angle of attack, α, and forward velocity, V (Ref. 24).

In the aforementioned tests on the VZ-4 and X-22A ducts (Refs. 21–24), the following characteristics of lip separation were observed:

- The onset of local flow separation on the lower lip rarely induced large changes in forces, moments, and power, but flow separation of the entire lower lip was accompanied by a rapid drop in pitching moment, an increase in power required to substantially greater than hover power, and increase in noise. Therefore, operation with full lower lip stall should be avoided.
- Propeller blade stresses remained well below critical even when the entire lower lip was stalled.

- Flow separation from the entire lower lip was found to be likely in descending flight conditions; i.e., conditions of low power and high duct angle of attack.
- Lip flow separation can be reduced to some extent by increasing the lip radius; however, there is a critical lip radius above which increasing the radius does not significantly delay separation (the critical lip radius is likely dependent on Reynolds number effects and duct diameter).
- Separation of the downstream (upper) lip was not accompanied by any detectable changes in forces, moments, and power, and no buffeting was evident; furthermore, stall of the downstream lip likely would not be encountered for the VTOL flight regime of the X-22A (Ref. 24).

Returning to the steady level flight transition regime that was determined in Ref. 22, Ref. 23 plotted the onset of lip stall with advance ratio, and determined that steady level flight without lip stall could be achieved for all forward flight velocities with a duct angle of attack margin of at least 8 degrees. Duct lip stall was also found not to limit maximum climb rate; however, duct lip stall did limit descent rate. Increasing the wing angle of attack increased the allowable descent rate because the wing provided additional lift and drag to enable operation of the duct at a reduced angle of attack. Therefore, a device that improves wing effectiveness in descent, for example, flap or droop, may improve descent rate capability. Devices that delay lip separation itself should also be considered, for example, vortex generators, active flow control, and/or variable lip geometry. For the first iteration of the tiltduct UAM reference vehicle discussed in this paper, transition and descent are not modeled, but it is assumed that devices to delay lip separation will be necessary; for example, on the X-22A, vortex generators were installed on the inner, lower lip of each duct (Ref. 25). Additionally, on the tiltduct UAM reference vehicle, a flap is placed along the main wing trailing edge. Other devices to improve wing effectiveness may be desirable after future analyses.

Acoustical Considerations

Ducts have the potential to reduce, shield and redirect noise. A number of high-level acoustical best practices and guidelines were incorporated in the design of the ducted proprotors, but detailed acoustical analyses were beyond the scope of this study. Future design studies targeting acoustic drivers may result in considerable modifications to the ducted proprotor geometry presented in this paper.

To maintain consistency with previous NASA UAM reference vehicles (Refs. 3, 6), the blade tip speed was kept below 550 ft/s due to a desire to reduce noise.

The placement and number of exit vanes inside the duct was driven somewhat by acoustical considerations. At this level of conceptual design, the specific geometry of the vanes was not precisely defined, but some rules of thumb were applied. The axial spacing between the proprotor and the vanes was targeted to be as large as practicable to reduce interaction noise. Additionally, the desired number of vanes was selected to avoid exciting the modes that propagate most efficiently in the duct at the blade passage frequency. Preliminary calculations were performed based on the duct diameter and proprotor blade count for the tiltduct reference vehicle by implementing methods described in Ref. 26, resulting in an estimate that the 8-bladed ducted proprotor should have five vanes, assuming that the vanes are evenly spaced. However, given that a horizontal exit vane is desired across the full duct diameter to aid in pitching moment control, implementation of 5 vanes will result in uneven vane spacing, and the influence of uneven vane spacing on acoustics should be considered in the future. Additional vane geometries may also influence acoustics, for example, angled or swept vanes.

Acoustic liners may be installed in the duct to further reduce noise radiation. Recent advances in liner design and fabrication, as demonstrated in Ref. 27 for example, indicate that it is possible to achieve low-frequency attenuation with the duct cross-sectional thicknesses expected of UAM vehicles. Acoustic liners were not implemented on this first iteration of the tiltduct UAM reference vehicle, but warrant further study.

Ducted Proprotor Geometry Selection

Designing novel ducted proprotors is a time consuming and costly process largely due to the required level of simulation fidelity. Currently, grid-based computational fluid dynamics (CFD) simulations are required to capture the complex flow physics between the tip of the proprotor and the inner diameter of the duct. Developing and running grid-based CFD models was beyond the scope of this work. Thus, duct design decisions were based on published experimental results.

The first design parameters considered were the duct area ratio, σ_d, and the duct chord length, l_{duct}. These two parameters are coupled due to the physics of the flow field inside of the duct. In order to capitalize on the duct performance benefits described in the "Ducted Proprotor Aerodynamics" section, σ_d should be maximized to reduce power consumption in hover, while l_{duct} should be minimized to reduce overall duct weight. However, if the diffuser ratio, σ_d / l_{duct}, is too large, then the slipstream inside of the duct could separate from the inner duct wall. If the flow is separated then the proprotor behaves similarly to an open rotor, and the power reduction benefit that the duct brings is negated. Based on the results reported in Ref. 28, in order to achieve a reasonable diffuser ratio, l_{duct} was selected to be equal to one rotor radius, and σ_d was varied from 1.0 to a maximum of 1.15 in later design trades.

The next parameter to be considered was related to proprotor chordwise location inside the duct. If the proprotor is located towards the leading edge of the duct, there is more axial distance available for diffusion of the flow, and the proximity to any exit vanes is reduced, reducing interference noise. On the other hand, if the proprotor plane is more rearward in the duct, proprotor asymmetric loading is reduced, minimizing blade stresses and associated noise during flight at non-zero angles

of attack. Reference 29 investigated a proprotor located at 25% and 40% of the duct chord length, measured from the duct leading edge, and saw that the proprotor at the rearward (40% chord) location may provide a small static thrust improvement, but a reduction in thrust during axial flight conditions. Additional studies are warranted at lower disk loadings that are more representative of UAM vehicles; for the tiltduct UAM reference vehicle, the proprotor chordwise location was set at 40% of the duct chord length.

Design of new proprotor blades was beyond the scope of this effort; the goal was simply to tune the NDARC model to obtain realistic proprotor performance characteristics. Therefore, proprotor blade parameters such as twist, chord, solidity, thickness, and sectional lift coefficients were taken from Ref. 28. To reduce blade loading while holding solidity constant, the number of blades was increased to eight, resulting in reduced blade chord. Reduced blade chord may reduce blade stiffness, but the effects of any changes in blade stiffness were beyond the scope of this study.

Duct positioning relative to the wing tip was intended to allow the duct support struts, about which the ducts tilt, to be extensions of each supporting wing's spar, and colocated with the exit vanes.

The final parameters considered were associated with the duct inlet lip shape and the centerbody shape; specific design of these geometries was not performed for this study, but some rules of thumb were considered. The duct inlet lip shape was assumed to be designed to minimize separation in hover while maintaining acceptable cruise drag. Future studies may determine that additional technologies are required in order to achieve a desired cruise speed; for example, variable inlet lip geometry. Meanwhile, the centerbody shape is recommended to be designed to minimize the rate of change of flow area at the diffuser inlet and thereby improve boundary layer characteristics and diffuser performance; for example, by locating the maximum centerbody cross-sectional area downstream of the minimum internal duct cross-sectional area (Ref. 14). A larger flow area at the proprotor also provides reduced through-flow velocities in the proprotor plane, improving proprotor efficiency.

Duct Aerodynamic Representation in NDARC

NDARC applies momentum theory to model ducted proprotor performance in axial flight. The current NDARC release does not, however, account for the additional circulation that exists on the duct itself when acting similar to an annular wing at a small angle of attack. To account for duct operations at small angles of attack, three NDARC wing components were added, one new wing for each pair of ducts[4]. The longitudinal locations of the newly added wings' aerodynamic centers were placed at the aerodynamic centers of the corresponding duct pair, and the added wings were represented by symmetric airfoils so that they only provide lift when operating at a non-zero angle of attack.

As discussed in the "Ducted Proprotor Aerodynamics" section, Ref. 20 tested an isolated duct with propeller blades removed and found that the duct produced approximately twice the lift of a rectangular wing with the same span and chord, and approximately equivalent induced drag. Given that the induced drag coefficient, C_{D_i}, of a rectangular wing is

$$C_{D_i} \propto \frac{{C_L}^2}{\pi \mathcal{AR}} \tag{6}$$

then, to represent the induced drag of a pair of ducts each with an aspect ratio of approximately two, a rectangular wing was used that had a span equal to two times the duct diameter and a chord equal to the duct chord length, and had twice the lift curve slope of a typical symmetric airfoil. The wing weights were negated by setting their NDARC tech factors equal to 0.0001, and these added wings influenced only the climb and cruise segments of the NDARC sizing mission.

Note that the present representation sums equivalent lift and induced drag as if the ducts and wings were in isolation; however, in reality, the ducts act somewhat as wing extensions, with complex flow at the wing tip, and the total lift and induced drag will not be a simple summation of the isolated wing and duct parameters. Future refinement of the model is warranted to improve estimation of lift and induced drag produced by the wing and ducted proprotor combined.

Duct Weight Estimation

The weight of a duct, W_{duct}, was estimated using the duct weight equation in NDARC (Ref. 7):

$$W_{duct} = \chi_{duct}(\pi d l_{duct}) U_{duct} \tag{7}$$

where χ_{duct} is a tech factor applied, $\pi d l_{duct}$ represents approximately half the wetted area of the duct, and U_{duct} is the duct weight per area.

A tech factor $\chi_{duct} = 0.65$ was used to be consistent with the tech factor used for wings on previous NASA tiltwing reference vehicles (Refs. 1,6). The duct weight per area $U_{duct} = 3.0$ lb/ft^2 was assumed to be equivalent to that of a secondary wing structure as defined in NDARC (a primary wing structure had a density of 5.0 lb/ft^2). Although the cylindrical duct shape may add some structural rigidity, the ducts are still required to tilt and provide lift, so U_{duct} should be revisited in future studies. No structural analyses were performed during this study; structural analyses are warranted in order to better estimate weight of the tilting ducts and their supporting wing and tail components.

Note that if duct chord length is kept proportional to diameter (l_{duct} was chosen to be equal to duct radius in the "Ducted Proprotor Geometry Selection" section), then for a fixed disk loading, the total weight, as estimated by Eq. 7, of all of the ducts on the vehicle would remain constant, even when the number of ducts is varied.

[4]The current release of NDARC is configured to incorporate up to eight wing components. Three wing components were already in use for the canard, main wing, and horizontal tail.

DESIGN REFINEMENT

Two different vehicle models were developed in NDARC to compare propulsion systems: a direct drive propulsion system and a cross-shafted propulsion system. A preliminary trade study was performed on each of the vehicle models to inform hover disk loading and duct area ratio choice, and then both models were tuned based on empirical tech factors.

The direct-drive propulsion system, depicted in Figure 6a, has a single gearbox which connects the turboshaft engine to the generator. The proprotors are directly connected to the output shafts of their respective electric motors. The cross-shafted propulsion system, depicted in Figure 6b, has four separate gear trains. Three of the gear trains connect a pair of electric motors to a pair of proprotors through a gearbox. For example, in Figure 6b, gearbox 1 connects electric motors 1 and 2 to proprotors 1 and 2. The fourth gear train in the cross-shafted propulsion system connects the turboshaft engine to the generator; the generator provides electrical power to the six electric motors. Note that the propulsion layout currently indicates that the spin directions of all proprotors on either the left or right of the vehicle are the same. Although this level of detail did not affect the NDARC sizing performed for this design study, a future trade study is warranted to determine the most appropriate spin directions; for example, with the current proprotor spin directions, a roll input during hover will induce a yaw moment.

After creating the two NDARC vehicle models, the design trade study varied hover disk loading, $\frac{T}{A_R}$, from 25 to 40 lb/ft^2, and duct area ratio, σ_d, from 1.0 to 1.15. Throughout the trade study, proprotor solidity was held constant and duct chord lengths were set equal to one rotor radius. Tables 2a and 2b display the gross weights of the direct-drive vehicle and the cross-shafted vehicle, respectively, for a specified duct area ratio and hover disk loading. From the trade study, a hover disk loading of 30 lb/ft^2 and duct area ratio of 1.15 were selected for both the direct-drive and cross-shafted vehicles. Note that with a hover disk loading of 35 lb/ft^2, both propulsion systems were lighter, but fuel burn increased by approximately 10%, so a hover disk loading of 30 lb/ft^2 assumed a reasonable compromise of efficiency and weight.

Table 2: Gross Weight (lb) at Specified Duct Area Ratios and Hover Disk Loadings, for Two Propulsion System Options

(a) Direct drive

Duct Area Ratio, σ_d	Hover Disk Loading, $\frac{T}{A_R}$ (lb/ft^2) 25	30	35	40
1.0	12070	7750	7420	8370
1.1	9120	7090	6850	7570
1.15	8660	6870	6640	7270

(b) Cross shafted

Duct Area Ratio, σ_d	Hover Disk Loading, $\frac{T}{A_R}$ (lb/ft^2) 25	30	35	40
1.0	7450	6620	6540	7090
1.1	6940	6200	6140	6640
1.15	6770	6060	6000	6460

One reason that NDARC is capable of modeling and sizing a wide variety of vehicles is the vast amount of model tuning available. Typically NDARC components, such as rotors, motors, or wings, will be tuned to match experimental data or higher fidelity models. The NDARC models for the tiltduct UAM reference vehicle, as far as applicable, utilized assumptions consistent with those for the six-passenger tiltwing UAM reference vehicle (Ref. 6). For the tiltduct, the wing weight model was set to the tiltrotor representation in NDARC. The wire weight model was set to the NDARC default; this wire weight model was developed during design of the six-passenger tiltwing UAM reference vehicle (Ref. 6). The ducted proprotors were modeled as ducted fan components in NDARC, and tuned as described in the remainder of this section.

One of the primary benefits of ducted proprotors is the inherent reduction of induced power for a particular thrust, relative to an identical open rotor. Incorporating this power reduction into the NDARC model for a ducted proprotor required adjustment of the rotor induced power multiplier for hover, $\kappa_{i_{hover}}$, and cruise, $\kappa_{i_{cruise}}$, where

$$P_i = \kappa_i P_{ideal}. \tag{8}$$

The induced power multipliers are used to account for effects of nonuniform inflow, non-ideal span loading, tip losses, swirl, blockage, and other phenomena (Ref. 5). To obtain reasonable power multipliers, NDARC was first run with the NDARC default values. Then, the output proprotor diameter, d, cruise velocity, V, and duct exit area, A_e, were utilized to calculate the thrust and power coefficients given an assumed figure of merit, η_{hover}, and cruise efficiency, η_{cruise}. The thrust coefficients were computed by

$$C_{T_{hover}} = \frac{T_{hover}}{\rho n^2 d^4} \tag{9}$$

and

$$C_{T_{cruise}} = \frac{T_{cruise}}{\rho n^2 d^4} \tag{10}$$

and the power coefficients were computed by

$$C^{est}_{P_{hover}} = \frac{d}{2\eta_{hover}\sqrt{A_e}} C^{3/2}_{T_{hover}} \tag{11}$$

and

$$C^{est}_{P_{cruise}} = \frac{C_{T_{cruise}}}{\eta_{cruise}} \left(\frac{V}{dn} \right). \tag{12}$$

Reference 24 found that both η_{hover} and η_{cruise} of about 80% were achievable, and so both efficiencies were set to 80% in

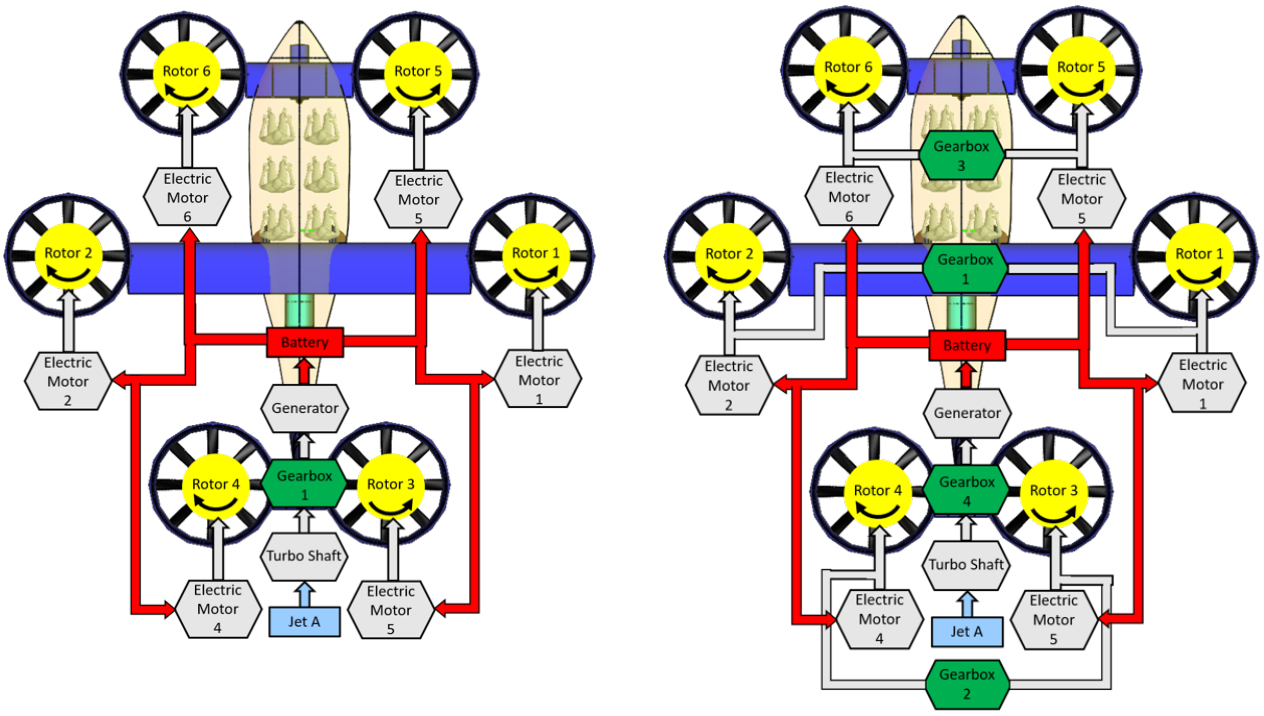

(a) Direct drive **(b) Cross shafted**

Figure 6: Propulsion layouts representing the two propulsion systems considered during design trades.

the NDARC model. With the power coefficients now computed, new NDARC multipliers were determined by

$$\kappa^k_{i_{hover}} = \frac{C^{est}_{P_{hover}} \kappa^{k-1}_{i_{hover}}}{C^{NDARC}_{P_{hover}}} \tag{13}$$

and

$$\kappa^k_{i_{cruise}} = \frac{C^{est}_{P_{cruise}} \kappa^{k-1}_{i_{cruise}}}{C^{NDARC}_{P_{cruise}}} \tag{14}$$

where the superscript k denotes the k^{th} iteration, and $C^{NDARC}_{P_{[*]}}$ is the induced power coefficient calculated by NDARC from the first step in this process. Because the updated $\kappa^k_{i_{[*]}}$ values depend on the NDARC model run with the previous multiplier ($\kappa^{k-1}_{i_{[*]}}$), this process is desired to be repeated until the percentage difference between iterations was $\leq 1\%$. During the model tuning, a new version of AIDEN was released that introduced a bug into AIDEN's N2 builder. The N2 builder allows users to automate processes and had been implemented to iterate the induced power multipliers. When this bug was discovered, a large number of changes had already been made to the vehicle models in the new AIDEN version, which were not directly compatible with the previous version, so the N2 builder was not used to tune the final vehicle model presented in this paper. The hover power coefficient was tuned manually to achieve a difference in iterations of $\leq 1\%$, equivalent to that which would be achieved with the N2 builder, and the final cruise power coefficient was within 10% of the value calculated with Equation 12.

The next NDARC multiplier adjusted was the tech factor applied to gearbox weights. NDARC tech factors function as constant multipliers to the NDARC calculated weights. The process to calculate the tech factor began by running NDARC with the default tech factor, to produce an initial gearbox weight and torque output by NDARC. The specific torque, ST, was computed using,

$$ST = \frac{\tau}{W^{NDARC}} \tag{15}$$

where τ is the maximum torque passed through the gearbox and W^{NDARC} is the gearbox weight. Next, the current ST was compared to the trend line of aircraft gearbox ST versus τ, which was generated in Ref. 30:

$$ST^{est} = 18.3\tau^{0.193} \tag{16}$$

where τ is the torque output by the initial NDARC run. Now plugging Equation 16 into Equation 15,

$$W^{est} = \frac{\tau^{0.807}}{18.3}. \tag{17}$$

The updated tech factor is calculated as a function of the previous NDARC outputs and the new W^{est},

$$\chi^k = \frac{W^{est}\chi^{k-1}}{W^{NDARC}}. \tag{18}$$

Again, the superscript k denotes the k^{th} iteration, and the convergence criteria set for these iterations was $\leq 1\%$ difference in χ between iterations.

Control surfaces were not modeled on this vehicle because of the difficulties associated with accurately capturing the flow physics inside of the ducts. Instead, the ducts were allowed to tilt in cruise to trim vehicle pitch. The maximum tilt angle utilized to trim the vehicle was approximately $\pm 1^{\circ}$. The relatively small corrections required for trimmed level flight should be easily achievable with internal duct control surfaces.

RESULTING TILTDUCT REFERENCE VEHICLE DESIGN

Both the direct-drive and cross-shafted NDARC models were tuned as discussed in the "Design Refinement" section of the paper, and the resulting OpenVSP, NDARC, and AIDEN models are available for download (Ref. 31). In an attempt to be representative of the UAM vehicle concepts proposed to date, the majority of which do not incorporate cross-shafted propulsion systems, the direct-drive vehicle was ultimately selected to be the first iteration of the NASA tiltduct UAM reference vehicle.

The direct-drive tiltduct vehicle resulting from the design process described in this paper is shown in hover and cruise modes in Figure 7, and Table 3 provides a comparison of performance parameters against the other NASA six-passenger UAM reference vehicles. Note that some of the technology assumptions used across the different UAM reference vehicles are not consistent at this time. Furthermore, it is important to note the limitations listed in the following subsection.

In Table 3, the single-main-rotor helicopter is denoted "SMR" and attributes are presented for the version with a main rotor tip speed of 550 ft/s. Propulsion systems include turboshaft ("TS"), fully electric ("E"), and turboelectric ("TE") and are either cross shafted ("CS") or direct drive ("DD"). The hover disk loading is defined as $\frac{T}{A_R}$. Note that the hover figure of merit is defined by the ratio of ideal power to actual power, where, for vehicles with open rotors, ideal power is obtained from momentum theory for an open rotor, and for the tiltduct vehicle, ideal power is obtained from momentum theory for a ducted rotor. The cruise wing area for the tiltduct vehicle accounts for duct wing area, calculated by multiplying the duct chord length by the duct diameter.

In comparing the hover figure of merit, cruise airspeed, energy burn, and power metrics presented in Table 3, the overall performance of the tiltduct is comparable with that of the tiltwing. At the current level of analysis, there are not obvious differences in performance that would specifically warrant a choice of the tiltduct over the tiltwing, or vice-versa. Therefore, other metrics may drive this choice; for example, ducts may provide improvements to the vehicle acoustic signature, improve safety during ground handling, or simply improve public perception due to the lack of open rotors.

In comparing the vectored thrust vehicles, i.e., the tiltduct and tiltwing, with the other six-passenger reference vehicles, it is evident that cruise and block speeds are higher for the vectored thrust vehicles. If the UAM business model is driven by passenger travel time savings, then this could be a key factor in vehicle selection.

There is scope for additional model tuning of the NASA UAM reference vehicles, trade studies on relevant technologies, and investigation of the sensitivity of the designs to alternative sizing missions representative of UAM operations. As future analyses and trade studies progress, the reference vehicles will be updated to improve the level of confidence in the predicted performance of the reference vehicles.

Limitations

The conceptual design of the tiltduct UAM reference vehicle described in this paper was performed based on information and data currently available. Importantly, the vehicle design is subject to a number of limitations as discussed in this section.

Beyond the basic aerodynamics models and tuning implemented in NDARC, no further aerodynamic modeling was performed. Additionally, the NDARC model neglected any interference of component slipstreams on any other components. Transition and descending flight were not modeled; however, rules of thumb were applied to the design based on historical data.

The historical data available for tilting ducted proprotors is almost entirely for disk loadings of greater than 100 lb/ft^2. The disk loading for this vehicle is significantly lower, 30 lb/ft^2, and therefore the applicability of the historical data to this vehicle is unknown. Of particular interest are the characteristics of low-disk-loading ducted proprotors at large angles of attack, and their influence on the vehicle's operational capabilities such as transition and descent corridors.

The specific duct geometry of this vehicle is not entirely defined; general attributes of the ducts were selected by reference to historical test data, and then performance of the ducts in the NDARC model was tuned to be realistic relative to the historical data. UAM vehicles with low disk loadings may need to incorporate additional technologies, such as variable geometry lips or flow control, in order to meet the hover, transition and cruise performance capabilities assumed in the design of this vehicle.

The proprotor implemented in this vehicle design has been tuned to achieve realistic performance characteristics relative to historical test data, but no targeted design of the proprotor blade geometry was performed.

Although some very basic acoustical considerations were made in the design of this vehicle, no acoustical analyses were performed. There is considerable scope for exploration into the potential for ducts to influence acoustics of UAM vehicles, and also to study how acoustic treatments may affect duct performance. Design of ducted proprotors for acoustics may produce duct characteristics very different than the ducts presented on this initial iteration of the NASA tiltduct UAM reference vehicle.

The tiltduct vehicle presented in this paper has a turboelectric powertrain for direct comparison with other NASA six-passenger UAM reference vehicles, which were designed for

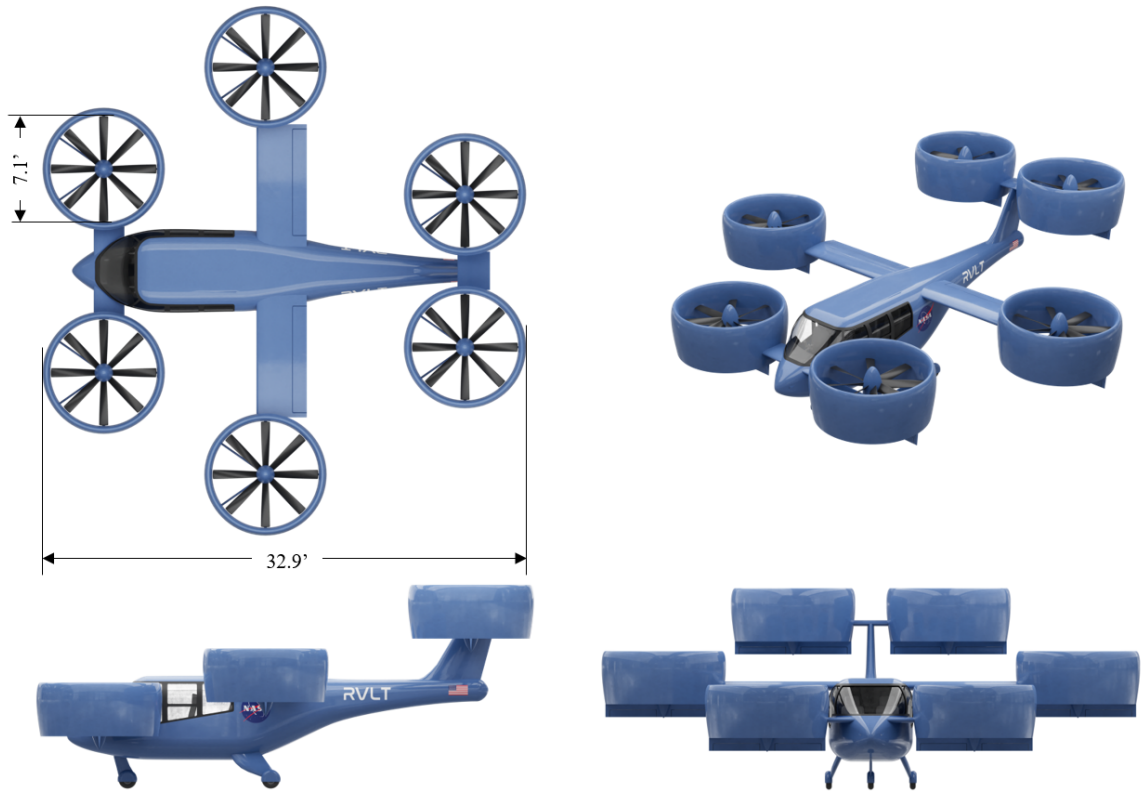

(a) Hover

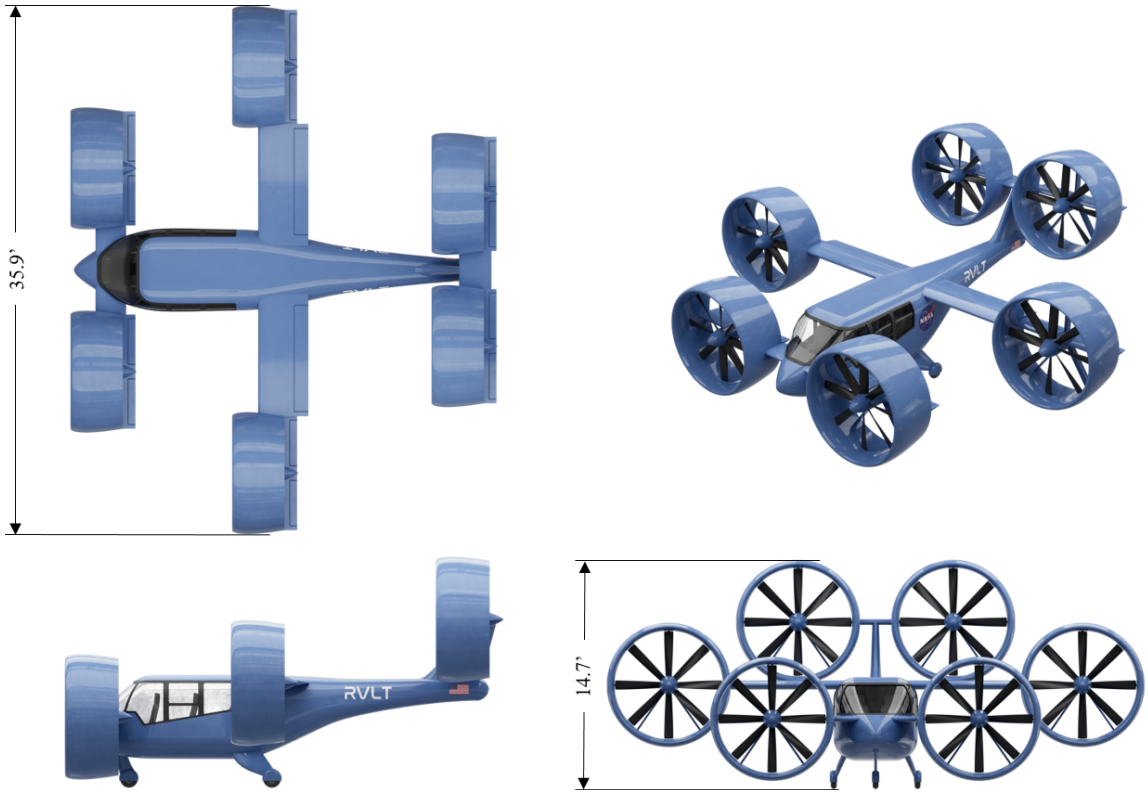

(b) Cruise

Figure 7: OpenVSP model representation of the tiltduct UAM reference vehicle design to date.

Table 3: Preliminary Comparisons of the Tiltduct Vehicle with Other Six-Passenger NASA UAM Reference Vehicles

Vehicle Configuration	Tiltduct	Tiltwing	Lift-plus-Cruise		Quadrotor		Side-by-Side		SMR
Propulsion System	DD TE	DD TE	DD TE	DD E	CS TS	CS E	CS TS	CS E	TS
Design gross weight (lb)	7089	6750	8190	8210	3740	6480	3470	4900	3740
(Prop)rotor diameter (ft)	7.08	7.33	10.0	10.0	18.4	26.2	21.0	29.8	34.5
Hover disk loading, $\frac{T}{A_R}$ (lb/ft^2)	30.0	20.0	13.1	13.1	3.50	3.00	5.00	3.50	4.00
Aircraft hover figure of merit	0.76	0.70	0.63	0.74	0.69	0.70	0.69	0.68	0.62
Cruise airspeed, V_{br} (kt)	151	148	128	112	122	98	116	98	102
Block speed (kt)	115	117	101	91.7	105	87.1	97	82.6	77.4
$L/D_e = WV_{br}/P$	9.1	8.7	7.9	8.5	4.9	5.8	5.9	7.2	5.4
Cruise wing area (ft^2)	229	128	256	275	N/A	N/A	21.3	42.9	N/A
Energy burn (MJ)	3170	3280	4260	1110	2670	1070	2210	686	2550
Weight/lift power (lb/hp)	7.32	6.03	6.65	7.40	12.8	14.0	10.7	12.6	10.5
Weight/cruise power (lb/hp)	19.6	20.3	22.5	24.9	13.1	18.4	16.9	24.4	16.9

the most constraining sizing mission presented in Ref. 2. Many industry UAM concepts propose a fully electric powertrain; it is recommended that future design trades on the tiltduct vehicle consider incorporating a fully electric powertrain and consider additional, less-constraining, sizing missions.

No structural analyses were performed. In particular, there is scope to improve the structural weight estimation of the tilting ducts and supporting wing and tail components.

CONCLUDING REMARKS

Based on this initial conceptual design of a six-passenger tiltduct reference vehicle for Urban Air Mobility, it is apparent that:

1. Vehicle performance alone is not likely to be a key driver in the selection of a tiltduct vehicle over a tiltwing vehicle, since no significant performance benefit is seen for the tiltduct reference vehicle relative to the tiltwing vehicle. Both vectored thrust vehicles achieve notably higher block speeds than the other reference vehicles.
2. Acoustical analyses were beyond the scope of this paper, but ducts have the potential to reduce, shield, and/or redirect noise. If ducts do indeed show significant improvements in acoustics, then acoustical priorities may provide a compelling reason to incorporate ducted proprotors on Urban Air Mobility aircraft.
3. If ducted proprotors are to be designed for Urban Air Mobility, then the acoustical and performance characteristics of ducted proprotors with low disk loadings and at large angles of attack, especially in descending flight and transition between cruise and hover modes, warrant significant further research. In particular, historical tests of tilting ducted proprotors were focused on VTOL operations at high disk loadings; Urban Air Mobility introduces new concepts of operation that may drive significantly reduced disk loading.

Author contact:
Siena K. S. Whiteside, siena.k.whiteside@nasa.gov.

ACKNOWLEDGMENTS

This work was funded by the NASA Aeronautics Research Mission Directorate through the Advanced Air Vehicle Program's Revolutionary Vertical Lift Technology Project. The authors would like to thank Kevin R. Antcliff and Nathan T. Crane for their involvement in early design trades, and Noah H. Schiller and Douglas M. Nark for their acoustics advice.

REFERENCES

1. Johnson, W., Silva, C., and Solis, E., "Concept Vehicles for VTOL Air Taxi Operations," AHS Technical Conference on Aeromechanics Design for Transformative Vertical Flight, San Francisco, CA, January 2018.

2. Patterson, M. D., Antcliff, K. R., and Kohlman, L. W., "A Proposed Approach to Studying Urban Air Mobility Missions Including an Initial Exploration of Mission Requirements," AHS International 74th Annual Forum & Technology Display, Pheonix, AZ, May 2018.

3. Silva, C., Johnson, W. R., Patterson, M. D., and Antcliff, K. R., "VTOL Urban Air Mobility Concept Vehicles for Technology Development," AIAA Aviation Technology, Integration, and Operations Conference, Atlanta, GA, June 2018.

4. Antcliff, K. R., Whiteside, S. K. S., Kohlman, L. W., and Silva, C., "Baseline Assumptions and Future Research Areas for Urban Air Mobility Vehicles," AIAA SciTech Forum, San Diego, CA, January 2019.

5. Johnson, W., "A Quiet Helicopter for Air Taxi Operations," VFS Aeromechanics for Advanced Vertical Flight Technical Meeting, San Jose, CA, January 2020.

6. Whiteside, S. K. S., Pollard, B. P., Antcliff, K. R., Zawodny, N. S., Fei, X., Silva, C., and Medina, G. L., "Design of a Tiltwing Concept Vehicle for Urban Air Mobility," NASA/TM-20210017971, NASA Langley Research Center, Hampton, VA, July 2021.

7. Johnson, W., "NDARC, NASA Design and Analysis of Rotorcraft, Theory, Release 1.15," Technical report, NASA Ames Research Center, Moffett Field, CA, October 2020.

8. Sinsay, J. D., Hadka, D. M., and Lego, S. E., "An Integrated Design Environment for NDARC," Aeromechanics for Vertical Lift Technical Meeting, San Francisco, CA, January 2016.

9. NASA, "OpenVSP," http://openvsp.org/, accessed 22 Nov 2021.

10. Python Software Foundation, "Python," https://www.python.org/, accessed 22 Nov 2021.

11. Kirk, J. V., Hall, L. P., and Hodder, B. K., "Aerodynamics of Lift Fan V/STOL Aircraft," AIAA 8th Annual Meeting and Technical Display, Washington, D.C., October 1971.

12. Nathen, P., "Architectural performance assessment of an electric vertical take-off and landing (e-VTOL) aircraft based on a ducted vectored thrust concept," Lilium GmbH, April 2021.

13. Schaefer, C. G., Jr., "XV-24A LightningStrike," AHS International 73rd Annual Forum and Technology Display, Fort Worth, Texas, May 2017, presentation.

14. Paxhia, V. B., and Sing, E. Y., "Design Development of a Dual Tandem Ducted Propeller VTOL Aircraft," IAS 31st Annual Meeting, New York, NY, January 1963.

15. Rankine, W. J. M., "On the Mechanical Principles of the Action of Propellers," *Transactions of the Institute of Naval Architects*, Vol. 6, April 1865, pp. 13–39.

16. Froude, R. E., "On the Part Played in Propulsion by Differences of Fluid Pressure," *Transactions of the Institute of Naval Architects*, Vol. 30, April 1889, pp. 390–405.

17. Kohlman, D. L., *Introduction to V/STOL Airplanes*, The Iowa State University Press, Ames, IA, 1981.

18. Leishman, J. G., *Principles of Helicopter Aerodynamics*, Cambridge University Press, December 2016.

19. Mort, K. W., "Performance Characteristics of a 4-Foot-Diameter Ducted Fan at Zero Angle of Attack for Several Fan Blade Angles," NASA TN D 3122, NASA Ames Research Center, Moffett Field, CA, December 1965.

20. Grose, R. M., "Wind Tunnel Tests Of Shrouded Propellers At Mach Numbers From 0 To 0.60," WADC TR 58-604, United Aircraft Corporation, Wright-Patterson Air Force Base, OH, December 1958.

21. Yaggy, P. F., and Goodson, K. W., "Aerodynamics of a Tilting Ducted Fan Configuration," NASA TN D 785, NASA Ames Research Center, Moffett Field, CA, March 1961.

22. Yaggy, P. F., and Mort, K. W., "A Wind Tunnel Investigation of a 4-Foot-Diameter Ducted Fan Mounted on the Tip of a Semispan Wing," NASA TN D 776, NASA Ames Research Center, Moffett Field, CA, March 1961.

23. Mort, K. W., and Yaggy, P. F., "Aerodynamic Characteristics of a 4-Foot-Diameter Ducted Fan Mounted on the Tip of a Semispan Wing," NASA TN D 1301, NASA Ames Research Center, Moffett Field, CA, April 1962.

24. Mort, K. W., and Gamse, B., "A Wind-Tunnel Investigation of a 7-Foot-Diameter Ducted Propeller," NASA-TN-D 4142, NASA Ames Research Center, San Jose, CA, August 1967.

25. Vertical Flight Society, "Bell X-22A," https://vertipedia-legacy.vtol.org/vstol/VSTOLWheel/BellX-22A.htm, accessed 22 Nov 2021.

26. Tyler, J. M., and Sofrin, T. G., "Axial Flow Compressor Noise Studies," SAE Technical Paper 620532, January 1962.

27. Nark, D. M., and Jones, M. G., "An Investigation of Bifurcation Acoustic Treatment Effects on Aft-Fan Engine Nacelle Noise," 25th AIAA/CEAS Aeroacoustics Conference, Delft, The Netherlands, May 2019.

28. Black, D. M., and Wainauski, H. S., "Hamilton Standard Shrouded Propeller Test Program, Vol I-IV," Technical Report HSER 4348, Hamilton Standard, Moffett Field, CA, May 1967.

29. Black, D., and Rohrbach, C., "Shrouded Propellers - A Comprehensive Performance Study," 5th AIAA Annual Meeting and Technical Display, Philadelphia, PA, August 1968.

30. Scheidler, J. J., Asnani, V. M., and Tallerico, T. F., "NASA's magnetic gearing research for electrified aircraft propulsion," AIAA/IEEE Electric Aircraft Technologies Symposium (EATS), Cincinnati, OH, July 2018.

31. NASA, "NASA UAM Reference Vehicles," https://sacd.larc.nasa.gov/rvlt, accessed 22 Nov 2021.